Hindawi
European Journal of Cancer Care
Volume 2024, Article ID 9712492, 12 pages
https://doi.org/10.1155/2024/9712492

Research Article

Integrated Analysis of a ceRNA (lncRNA-miRNA-mRNA) Regulatory Network for Prostate Cancer

Hongliang Wu, Sheng Wang, Zhijun Chen, Shuai Yang, Wenyan Sun, and Han Guan

Department of Urology, First Affiliated Hospital of Bengbu Medical College, Bengbu, China

Correspondence should be addressed to Han Guan; gh668689@126.com

Received 28 May 2023; Revised 20 December 2023; Accepted 1 February 2024; Published 23 February 2024

Academic Editor: Mohammad Reza Kalhori

Copyright © 2024 Hongliang Wu et al. This is an open access article distributed under the Creative Commons Attribution License, which permits unrestricted use, distribution, and reproduction in any medium, provided the original work is properly cited.

Objective. This study was to construct a ceRNA (lncRNA-miRNA-mRNA) regulatory network for prostate cancer (PCa) and to explore the prognostic correlation, key biological functions, and pathways of core RNAs. *Methods*. Three subgene expression matrices (miRNA, lncRNA, and mRNA expression matrix) were taken from the TCGA database and used in this investigation. Differential expression analysis and differential expression miRNAs were carried out. Next, the ceRNA (lncRNA-miRNA-mRNA) regulatory complex was used to visualize our data and show how they interacted. Ultimately, the primary molecular roles and biological pathways of PCa were identified using enrichment analysis by the Kyoto Encyclopedia of Genes and Genomes (KEGG) and Gene Ontology (GO). An effect of AC016773.1 on prostate cancer cell proliferation was investigated by knocking out AC016773.1 in an animal model. The interrelationship between AC016773.1 and hsa-mir-25 was validated using RNA immunoprecipitation technology. *Results*. The lncRNA, miRNA, and mRNA expression matrices obtained from the TCGA database contain 16901, 1881, and 19962 transcripts, respectively. Through differential expression analysis, we obtained 2010 de lncRNA comparative information, 75 lncRNA and miRNA interaction pairs, and 31 targeted de mRNAs. Through the differential expression analysis of RNA nodes in the ceRNA regulatory network, we found that compared with the NP group, in the PCa group, there were 14 lncRNAs upregulated and 25 lncRNAs downregulated, 1 miRNA upregulated and 3 miRNA downregulated, and 10 mRNA upregulated and 21 mRNA downregulated. In KEGG enrichment analysis, the pathways identified by targeted DE-mRNAs were mainly related to calcium signaling pathway, EGFR tyrosine kinase inhibitor resistance, melanoma, PI3K–Akt signaling pathway, and proteoglycans in cancer. In animal models, it was found that knocking down AC016773.1 significantly reduced tumor volume and weight, indicating that AC016773.1 may promote the proliferation of PCa cells. The use of RNA immunoprecipitation technology indicates a direct binding between AC016773.1 and hsa-mir-25. *Conclusion*. We elucidated the network regulatory relationship of lncRNA-miRNA-mRNA in PCa and further explored the key molecular functions, biological pathways, and prognostic value of targeted DE-mRNAs.

1. Introduction

Prostate cancer (PCa) is an epithelial tumor occurring in the prostate and is the most common malignancy of the male genitourinary system. The incidence of PCa is extremely high in older men, with 80% of cases occurring in men over 65 years of age, accounting for about 13.5% of male malignancies [1, 2]. The causative factors of PCa are not fully understood and may be related to age, race, genetics, environment, food, obesity, and sex hormones [3, 4]. Most of the early PCa has no obvious symptoms. With the growth of the tumor, PCa can be manifested as lower urinary tract obstruction symptoms, such as frequent urination, urgent urination, slow urine flow, strenuous urination, and even urinary retention or incontinence. Prostate cancer cells can spread to other parts of the body, including pelvic and retroperitoneal lymph nodes, spinal cord, bladder, rectum, and bone metastases. When bone metastases occur, they can cause symptoms such as bone pain, spinal cord compression, and pathological fractures [5, 6]. Clinical diagnosis is often made by digital rectal examination (DRE), prostate-specific antigen (PSA) test, rectal ultrasound, and puncture biopsy

[7]. At present, radical resection of PCa is the most effective way to treat PCa. After standard treatment, the prognosis of PCa is generally good [8].

The miRNAs are important regulators of biological processes in PCa progression. MicroRNAs (miRNAs) are a class of endogenous noncoding RNAs with regulatory functions found in eukaryotes. They are about 20 to 25 nucleotides in length [9]. They recognize targeted mRNAs through base complementary pairing and degrade targeted mRNAs or inhibit their translation [10] while long noncoding RNAs (lnRNAs) act as miRNA sponges, which can specifically adsorb a large number of miRNAs and competitively bind miRNAs to mRNAs, thus playing a regulatory role in life activities [11]. Messenger RNA (mRNA) is a type of single-stranded ribonucleic acid that is transcribed from a strand of DNA as a template and carries genetic information to guide protein synthesis.

In the present study, we sorted out and obtained subgene expression matrixes of lncRNA, miRNA, and mRNA and performed differential expression analysis to identify differentially expressed lncRNAs (DE-lncRNAs), miRNAs (DE-miRNAs), and mRNAs (DE-mRNAs) between PCa and normal control (NC) groups. Then, we identified the comparison relationships between DE-lncRNAs and DE-miRNAs and targeted DE-mRNAs in PCa samples. Next, we constructed a ceRNA (lncRNA-miRNA-mRNA) regulatory network and analyzed the differential expression of RNAs in the regulatory network and the correlation between survival and prognosis. Finally, GO function and KEGG pathway enrichment analyses of mRNAs in PCa were performed.

2. Materials and Methods

2.1. Cell Source and Culture Condition. The Cell Bank of Type Culture Collection of the Chinese Academy of Sciences is the source of the human normal prostate epithelial cell line (RWPE1), 293T cells, and PCa cell lines (DU145 and PC3). The keratinocyte-serum-free media that were used to cultivate RWPE1 cells contained 5 ng/ml of epidermal growth factor and 0.05 mg/ml of bovine pituitary extract (both obtained from Gibco, Thermo Fisher Scientific, Inc.). Invitrogen (Thermo Fisher Scientific, Inc.) was used to cultivate PC3 and 293T cells, while RPMI 1640 media (Invitrogen) was used to sustain DU145 cells. All culture media were enriched with 10% FBS (Gibco; Thermo Fisher Scientific, Inc.) and 1% penicillin/streptomycin (Sigma Aldrich; Merck KGaA). Every cell was kept in a 37°C, 5% CO2 humidified environment.

2.2. Download and Arrangement of Transcriptome Expression Matrix. The collaboration of the National Cancer Institute and the National Human Genome Research Institute creates the Cancer Genome Atlas (TCGA) database as part of a cancer research effort. The TCGA database is now our primary choice for cancer research because of its enormous sample size, variety of data sources, and standard format [12]. We obtained the subgene expression matrix of lncRNA, miRNA, and mRNA, respectively, by sorting through the entire transcriptome expression matrix of PCa that we had acquired from the TCGA database.

To find differentially expressed mRNAs (DE-mRNAs), miRNAs (DE-miRNAs), and lncRNAs (DE-lncRNAs) across PCa and NC groups, differential expression analysis was conducted. To compare the three types of RNAs expression levels between the PCa group and the NC group, the subgene expression matrices of miRNAs, lncRNAs, and mRNAs were entered into the R software, respectively, and referred to the R package limma. The data were then visualized using the R package pheatmap [13, 14].

2.3. Analysis of the Sequence Alignment between DE-miRNAs and DE-lncRNAs. After downloading the lncRNAs and miRNAs comparison files from the miRcode database (https://www.mircode.org/), we used a specially created Perl script to get the comparative data for every DE-lncRNA. The comparison relationship between DE-lncRNAs and DE-miRNAs in PCa samples was established by reading the list of DE-miRNAs [15, 16].

2.4. Determination of the Intended DE-mRNAs. Then, using the starBase database (https://starbase.sysu.edu.cn), precursor DE-miRNAs were labeled 3p or 5p, and candidate DE-miRNAs-targeted mRNAs were sourced from the miRDB (https://www.mirdb.org/), miRTarBase (https://mirtarbase.mbc.nctu.edu.tw/), and TargetScan databases (https://www.targetscan.org/) [17, 18]. We categorized the mRNAs as targeted mRNAs of PCa if the mRNAs were predicted in all three databases to be DE-miRNAs-targeted mRNAs. Ultimately, tailored DE-mRNAs were obtained by performing the intersection of targeted mRNAs and DE-mRNAs.

2.5. Establishment of a ceRNA (lncRNA-miRNA-mRNA) Regulatory Complex. The interaction matrixes between DE-mRNAs and DE-miRNAs and between DE-lncRNAs and DE-miRNAs were calculated and obtained using custom Perl scripts, and the attributes of each RNAs (upregulated or downregulated expression in the PCa group and which type of RNAs belong to) were collated and labeled. The ceRNA (lncRNA-miRNA-mRNA) regulatory complex was visualized by the software Cytoscape [19].

2.6. RNA Differential Expression Analysis in ceRNA Regulatory Networks. We input the list of miRNAs, lncRNAs, and mRNAs that constituted the ceRNA regulatory network into R software and extracted their expression values in different grouped samples according to the transcriptome expression matrix. Then, we referred to the R package pheatmap and defined the bioheatmap to draw the gene expression heatmap and visualize the miRNAs, lncRNAs, and mRNAs expressions in the ceRNA regulatory network [20, 21].

2.7. Survival Analysis of ceRNA Regulatory Network. We performed survival analyses of DE-miRNAs, DE-lncRNAs, and DE-mRNAs involved in the construction of the ceRNA regulatory complex, respectively, to evaluate the effectiveness of different RNA expression levels on the survival prognosis of PCa patients [22]. First, we sorted out the survival time and survival state of PCa patients, and then compared the survival differences of patients with three types of different RNAs with different expression levels by using R package survival, and drew survival curves to visualize the results [23].

2.8. Analysis of mRNA Function and Pathway Enrichment in PCa. We may learn more about the molecular role and biological route of mRNAs by examining KEGG and GO enrichment [24]. With the help of R packages clusterProfiler, org.Hs.eg.db, enrichment plot, and ggplot2, we first carried out GO enrichment analysis of mRNAs, covering cellular components (CC), biological processes (BP), and molecular functions (MF). Subsequently, KEGG enrichment analysis of mRNAs was performed by the function enrich KEGG owing to determine the main molecular biological pathways of PCa [25, 26]. Ultimately, the enrichment results were visualized.

2.9. Subcutaneous PCa Models in Naked Mice. The Animal Care and Use Committee of Bengbu Medical College approved the protocol and procedures for all animal experiments. Shanghai GenePharma Co. Ltd. created the pGPH1-short hairpin RNA (shRNA) plasmids to knockdown AC016773.1 (sh-AC016773.1 or sh-NC). PC3 cells were transfected with 2 μg of sh-AC016773.1 or sh-NC plasmids at room temperature using Lipofectamine® 2000 (Thermo Fisher Scientific, Inc.). 48 more hours were spent incubating the cells. To create a stable AC016773.1-knockdown PC3 cell line, 2 mg/ml neomycin was then given to PC3 cells following transfection with sh-AC016773.1 or sh-NC for two to three weeks. s.c. injection of PC3 cells (1×106 cells in 100 μl PBS) transfected with shRNA-AC016773.1 or control shRNA was used to create PCa xenograft models.

The animals were kept in housing with a 12-hour light-dark cycle, continuous humidity (40–70%) with unrestricted food and water. Fifteen mice in all were acquired; three were withdrawn from the experiment because two of the animals passed away during anesthesia and one died before subcutaneous injection (the cause of death was not determined by autopsy). Twelve mice remained, and they were split randomly into two groups (shRNA-NC or shRNA-AC016773.1; $n = 6$ per group). Every four days, the weight of the mice and their condition were observed. The following humane endpoints were used to decide when an animal needed to be put to sleep: 20–25% of the animal's initial body weight lost; 24-hour appetite loss; serious illness; tumor growth exceeding 10% of the animals that are weak or near death; and the original body weight or the average diameter greater than 20 mm.

All 12 tumor-bearing mice survived 28 days of subcutaneous injections before being put to death by an i.p. injection of 0.7% pentobarbital sodium (150 mg/kg) to induce extreme anesthesia. Tumor samples were removed and weighed when the mice passed away, which was verified by respiratory arrest and cardiac arrest lasting more than two minutes. We measured the width and length of the tumor. The formula used to compute the tumor volume was $V = (\text{length} \times \text{width2})/2$.

2.10. RIP Assay. The Magna Nuclear RIPTM (Cross-Linked) Nuclear RNA-Binding Protein Immunoprecipitation Kit (EMD Millipore) was used based on the instructions of the manufacturer. Further being transfected with the specified genes, PC3 cells (2×107) were collected and lysed on ice. Proteins and RNAs were crosslinked by incorporating 37% formaldehyde and letting it sit at room temperature for ten minutes. Glycine was used to remove extra formaldehyde, and cell pellets were centrifuged at $800 \times g$ for five minutes at 4°C. The nuclei isolation buffer was then incorporated into the cell pellets and incubated for 15 minutes on ice.

The cross-linked proteins and RNAs were then released by adding RIP cross-linked lysis buffer. The sample was subjected to five 50% power pulses with a 30-second gap between each pulse using the SM-250D (Nanjing Shunmao Technology Co., Ltd.) sonicator. At all times, the tubes were kept chilled on ice. To obtain conjugated beads, protein A/G magnetic beads (supplied in the kit) were incubated with specific argonaute RNA-induced silencing complex (RISC) catalytic component 2 (GOLM1; cat. no. MA5-14861; 1: 10; Thermo Fisher Scientific Inc.) or IgG antibodies (cat. no. PP64B; 1: 10; EMD Millipore) at 4°C for approximately three hours and incubated at 4°C after combining the conjugated beads with sonicated lysis. After three hours, the beads were cleaned with ice-cold low-salt wash buffer. Proteinase K was used to extract the protein from the beads. Lastly, the AC016773.1 or hsa-mir-25 existence in immunoprecipitated RNA was examined by qPCR.

3. Results

3.1. RNA Expression Matrixes and PCa Patient Information. We obtained the whole-transcriptome expression matrix of PCa from the TCGA database and obtained three subgene expression matrices (lncRNA, miRNA, and mRNA expression matrices), which contained 16901, 1881, and 19962 transcripts, respectively. There were 492 samples in the PCa group and 51 in the normal untreated (NU) group. For details, see Supplementary Document 1.

3.2. Identification of DE-lncRNAs, DE-miRNAs, and DE-mRNAs between PCa and NC Groups. We conducted differential expression analysis of lncRNA, miRNA, and mRNA expression matrixes, respectively, and the results showed that there were 415 upregulated and 637 downregulated DE-

lncRNAs, 13 upregulated and 19 downregulated DE-miRNAs, and 904 upregulated and 1423 downregulated DE-mRNAs, in the PCa group compared to NC. We used heatmaps to show the top 20 DE-RNAs with the most significant upregulated and downregulated expression of three kinds of RNA (Figures 1(a)–1(c)). According to the adjust P value <0.05 and $|\text{lgFC}| \geq 1$, there was a statistically significant difference.

3.3. Identification of lncRNA-miRNA Interaction Pairs and Targeted DE-mRNAs. We obtained 2010 DE-lncRNAs comparison information and 75 lncRNAs and miRNAs interaction pairs through the miRcode database and Perl script (see Supplement 2 for details). In addition, 364 targeted mRNAs were obtained from the aforementioned database, and 2327 DE-mRNAs were obtained by differential expression analysis. After taking their intersection, 31 targeted DE-mRNAs were finally obtained (as shown in Figure 2).

3.4. The ceRNA (lncRNA-miRNA-mRNA) Regulatory Network of PCa. We obtained 34 pairs of DE-mRNAs and DE-miRNAs and 75 pairs of DE-lncRNAs and DE-miRNAs by Perl script (see Supplement 3 for details). The interactions between them were visualized through the ceRNA (lncRNA-miRNA-mRNA) regulatory network (as shown in Figure 3).

3.5. Differential Expression of lncRNAs, miRNAs, and mRNAs in the ceRNA Regulatory Network. LncRNAs, miRNAs, and mRNAs participating in the construction of the ceRNA regulatory network were, respectively, analyzed for differential expressions to visually represent their differential expression in the PCa group and NC group samples, as shown in Figure 4. Compared with the NP group, in the PCa group, there were 14 lncRNAs upregulated and 25 lncRNAs downregulated (Figure 4(a)), 1 miRNA upregulated and 3 miRNA downregulated (Figure 4(b)), and 10 mRNA upregulated and 21 mRNA downregulated (Figure 4(c)).

3.6. Survival Curves of High and Low Expression RNAs in the ceRNA Regulatory Network. We compared the survival differences between PCa patients with high expression and low expression of lncRNAs, miRNAs, and mRNAs in the ceRNA regulatory network and plotted survival curves. As shown in Figure 5, the survival rates of patients with high expression groups of AC016773.1, EZH2, GOLM1, and hsa-mir-25 were significantly lower than those of the low expression groups ($P < 0.05$), while the survival rates of patients with low expression groups of AC127496.3 and C8orf31 were significantly lower than those of the high expression groups ($P < 0.05$).

3.7. GO and KEGG Enrichment of 31 Targeted DE-mRNAs in PCa. PCa's key molecular functions and biological pathways were uncovered using GO and KEGG enrichment analysis. GO enrichment analysis showed that the functions of BP mainly included inositol lipid-mediated signaling, phosphatidylinositol 3-kinase signaling, phosphatidylinositol-mediated signaling, positive regulation of MAP kinase activity, and positive regulation of phosphatidylinositol 3-kinase signaling (Figure 6(a)). The function of CC is closely related to the asymmetric synapse, cis-Golgi network, neuron-to-neuron synapse, postsynaptic density, and postsynaptic specialization (Figure 6(b)). The functions of MF mainly focus on calcium channel activity, calcium-release channel activity, inositol 1,4,5 trisphosphate binding, intracellular ligand-gated ion channel activity, and ligand-gated calcium channel activity (Figure 6(c)). In KEGG enrichment analysis, targeted DE-mRNAs identified pathways mainly focused on calcium signaling pathway, EGFR tyrosine kinase inhibitor resistance, melanoma, PI3K−Akt signaling pathway, and proteoglycans in cancer (Figure 6(d)).

3.8. Nude Mouse PCa Subcutaneous Models. With the aim of investigating the effects of AC016773.1 on prostate tumor growth in vivo, we subjected the PC-3 cells with a stable AC016773.1 knockdown to nude mice, and these tumor cells formed a relatively obvious tumor cell mass (Figure 7(a)). Animal models were established via subcutaneous injection of control shRNA-treated or shRNA-AC016773.1-treated PC3 cells in male nude mice. Research has found that knocking down the AC016773.1 genome did not result in significant weight loss compared to the sh-NC group (Figure 7(b)) but significantly reduced tumor volume and weight in the nude (Figure 7(c)). These results indicate that knocking out AC016773.1 can inhibit the growth of PCa tumors in vivo.

3.9. RIP Assay. Following a suggestion that AC016773.1 might be an oncogene, its mode of action was looked into. The majority of AC016773.1 was found to be in the cytoplasm. It has been suggested that via sponging miRNAs in human cancer, lncRNAs may take place a vital role in the posttranscriptional control of mRNAs. A human miRNA target tool (DIANA tools) was used to predict putative miRNA binding sites in AC016773.1. HSA-mir-25 binding sites were found. As a result, hsa-mir-25 was the focus of the current study's examination. After AC016773.1 was knocked down, there was a notable rise in hsa-mir-25 expression.

On the other hand, hsa-mir-25 expression was reduced by AC016773.1 overexpression. In PCa cells, AC016773.1 and hsa-mir-25 bind to GOLM1. By attaching to GOLM1, miRNAs create a functioning RISC that aids in the degradation of mRNAs by the RISC, hence executing their gene-silencing function. PC3 cell extracts were used for anti-GOLM1 RIP in order to confirm the current theory. The presence of hsa-mir-25 and AC016773.1 in the immunoprecipitates was assessed using RT-qPCR.

In comparison to the anti-IgG control, AC016773.1 was enriched in anti-GOLM1 conjugated immunoprecipitates. Hsa-mir-25 was also consistently found in the immunoprecipitates (Figure 8). Thus, GOLM1 probably used direct binding to pull down both AC016773.1 and hsa-mir-25.

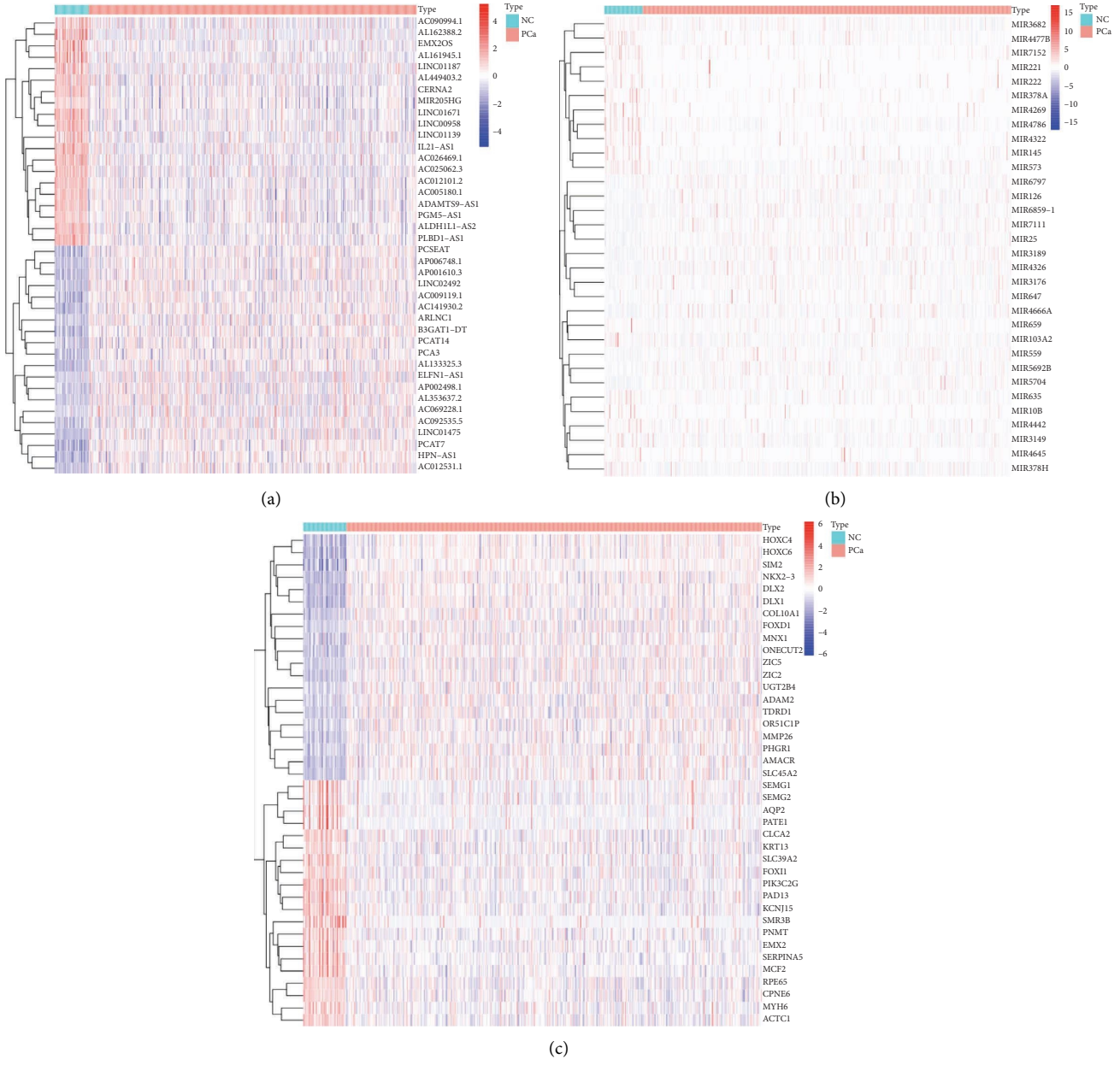

Figure 1: Differential expression of genes in PCa compared to the control group. The heatmaps of DE-lncRNAs (a), DE-miRNAs (b), and DE-mRNAs (c) expressed in PCa. Red squares indicate upregulated RNAs; blue squares indicate downregulated RNAs.

Overall, the current investigation revealed the reciprocal relationship between AC016773.1 and hsa-mir-25 and recommended that there was direct binding among the two.

4. Discussion

PCa is a kind of tumor caused by malignant hyperplasia of prostate epithelial cells, often manifested as abnormal urination, pelvic discomfort, erectile dysfunction, and so on, and is not infectious but has a certain genetic tendency [27, 28]. Therefore, through comprehensive bioinformatics analysis, this paper discussed the core pathogenic genes of PCa and their key biological functions and important pathways. In this study, we obtained three subgene expression matrices (lncRNA, miRNA, and mRNA expression matrices) from the TCGA database, which contained 16901, 1881, and 19962 transcripts, respectively. Differential expression analysis showed that there were 415 upregulated and 637 downregulated DE-lncRNAs, 13 upregulated and 19 downregulated DE-miRNAs, and 904 upregulated and 1423 downregulated DE-mRNAs. We then obtained 2010 DE-lncRNAs comparison information, 75 lncRNAs and miRNAs interaction pairs, and 31 targeted DE-mRNAs. Next, we gained 34 pairs of DE-mRNAs and DE-miRNAs and 75 pairs of DE-lncRNAs and DE-miRNAs. Also, the interactions between them were visualized through the ceRNA (lncRNA-miRNA-mRNA) regulatory network. Through the differential expression analysis of RNA nodes in

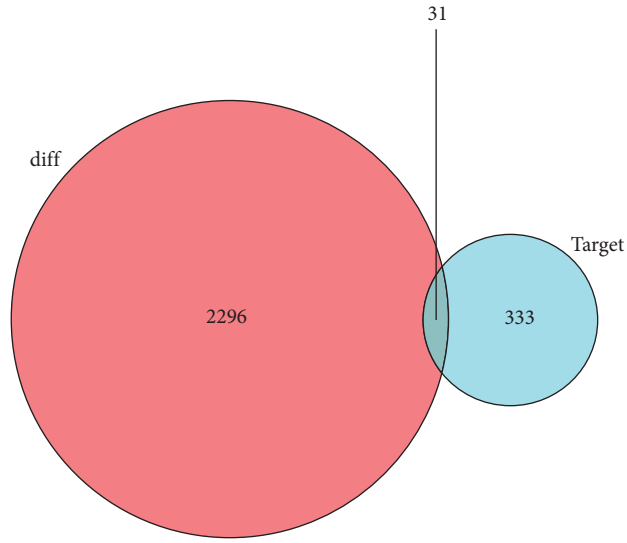

Figure 2: The Venn diagram of targeted DE-mRNAs was screened by sequence alignment analysis and differential expression analysis. The red circular area represents DE-mRNAs, the blue circular area represents targeted mRNAs, and the intersection area represents targeted DE-mRNAs.

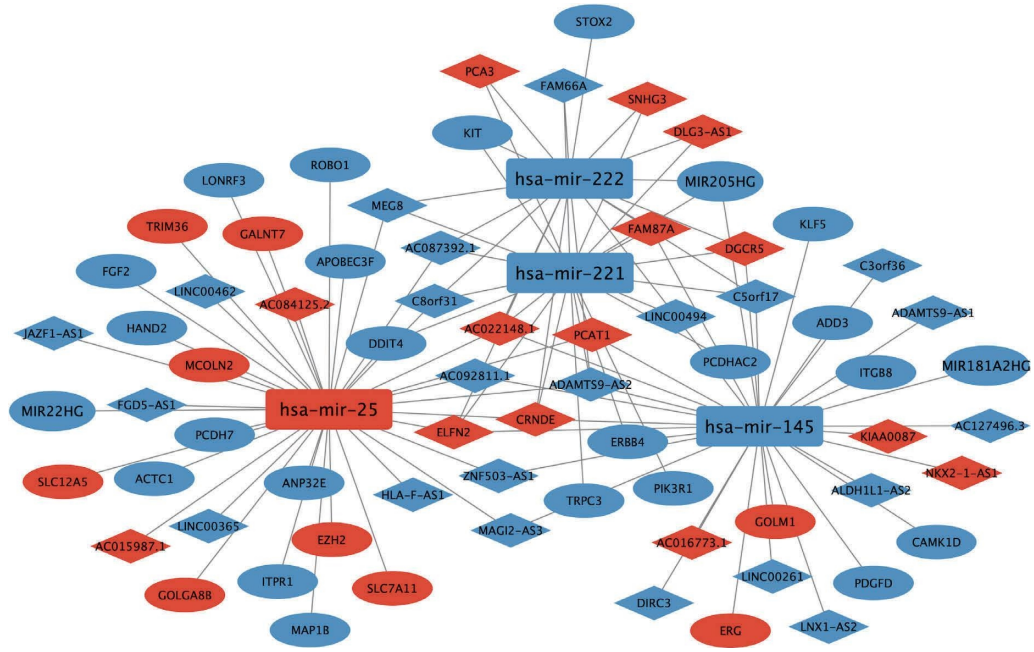

Figure 3: The ceRNA (lncRNA-miRNA-mRNA) regulatory network of PCa. Rectangular nodes represent miRNAs, oval nodes represent mRNAs, and diamond nodes represent lncRNAs. Red indicates upregulated expression, and blue indicates downregulated expression; the lines between them represent the interactions between different types of RNAs.

the ceRNA regulatory network, we found that compared with the NP group, in the PCa group, there were 14 lncRNAs upregulated and 25 lncRNAs downregulated, 1 miRNA upregulated and 3 miRNA downregulated, and 10 mRNA upregulated and 21 mRNA downregulated. In addition, the survival analysis curves showed that the survival rates of patients with high expression groups of AC016773.1, EZH2, GOLM1, and hsa-mir-25 were significantly lower than those of the low expression groups ($P < 0.05$), while the survival rates of patients with low expression groups of AC127496.3 and C8orf31 were significantly lower than those of the high expression groups ($P < 0.05$). Finally, GO and KEGG enrichment analysis revealed the key molecular functions and biological pathways of PCa. For example, GO enrichment analysis showed that the functions of targeted DE-mRNAs mainly focus on phosphatidylinositol 3-kinase signaling, positive regulation of MAP kinase activity, cis-Golgi network, neuron-to-neuron synapse, calcium channel activity, and inositol 1,4,5 trisphosphate binding. In KEGG enrichment analysis, the pathways identified by targeted DE-

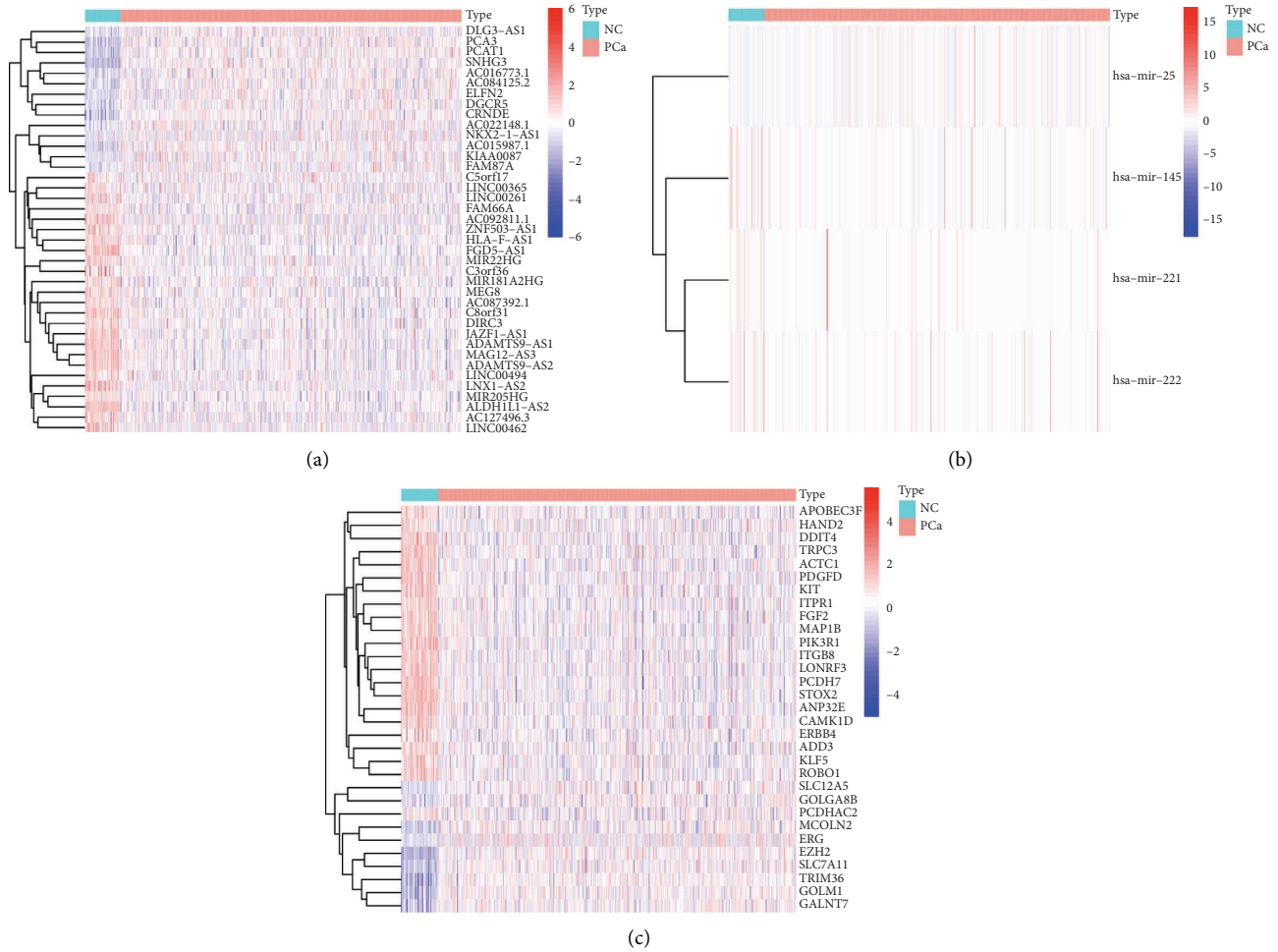

Figure 4: Differential expression of genes in PCa compared to the control group. The heatmaps of lncRNAs (a), miRNAs (b), and mRNAs (c) expressions involved in the ceRNA regulatory network of PCa. Red squares indicate upregulated RNAs; blue squares indicate downregulated RNAs.

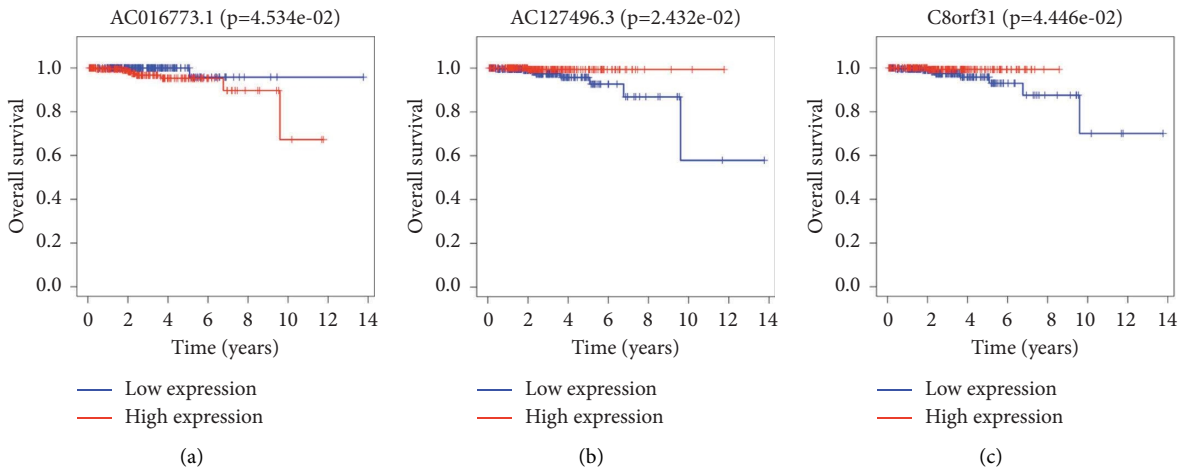

Figure 5: Continued.

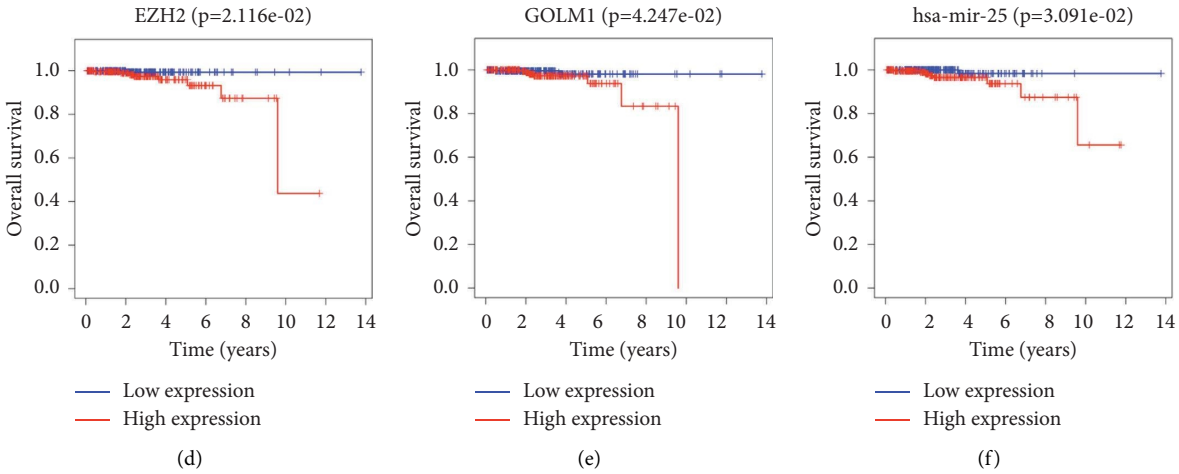

Figure 5: Survival curves of high and low expression groups of different RNAs. Abscissa, survival years; ordinate, overall survival rate. (a) AC016773.1, (b) AC127496.3, (c) C8orf31, (d) EZH2, (e) GOLM1, and (f) hsa-mir-25.

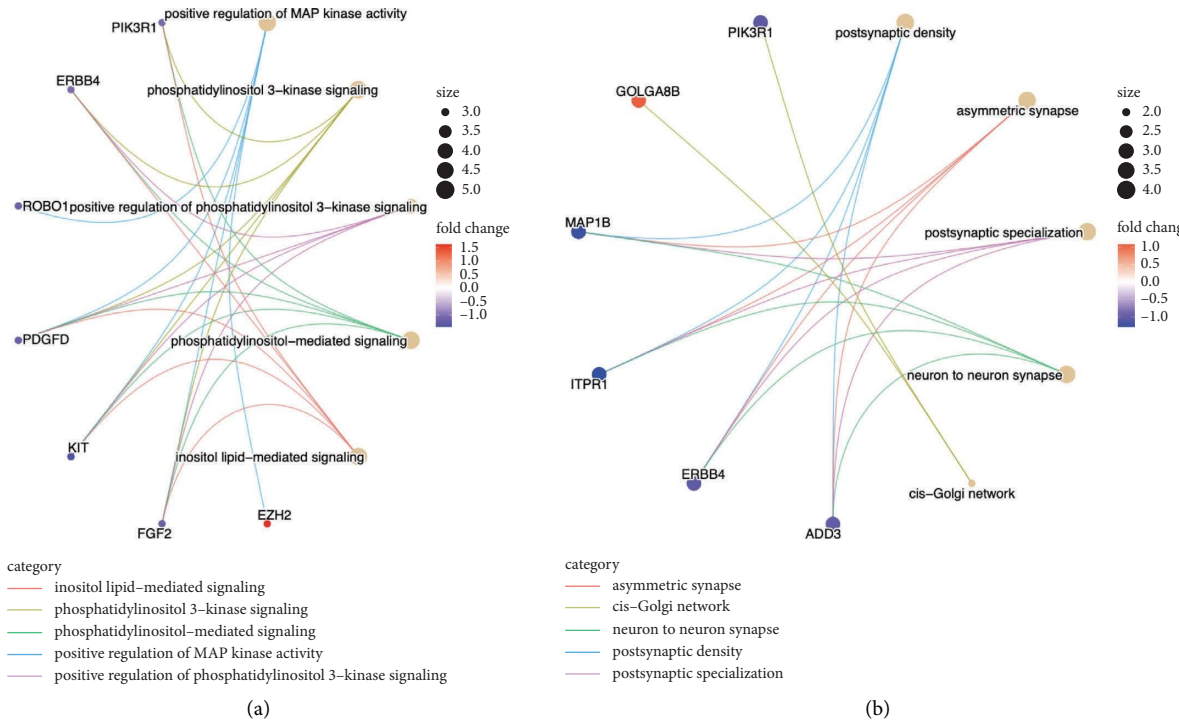

Figure 6: Continued.

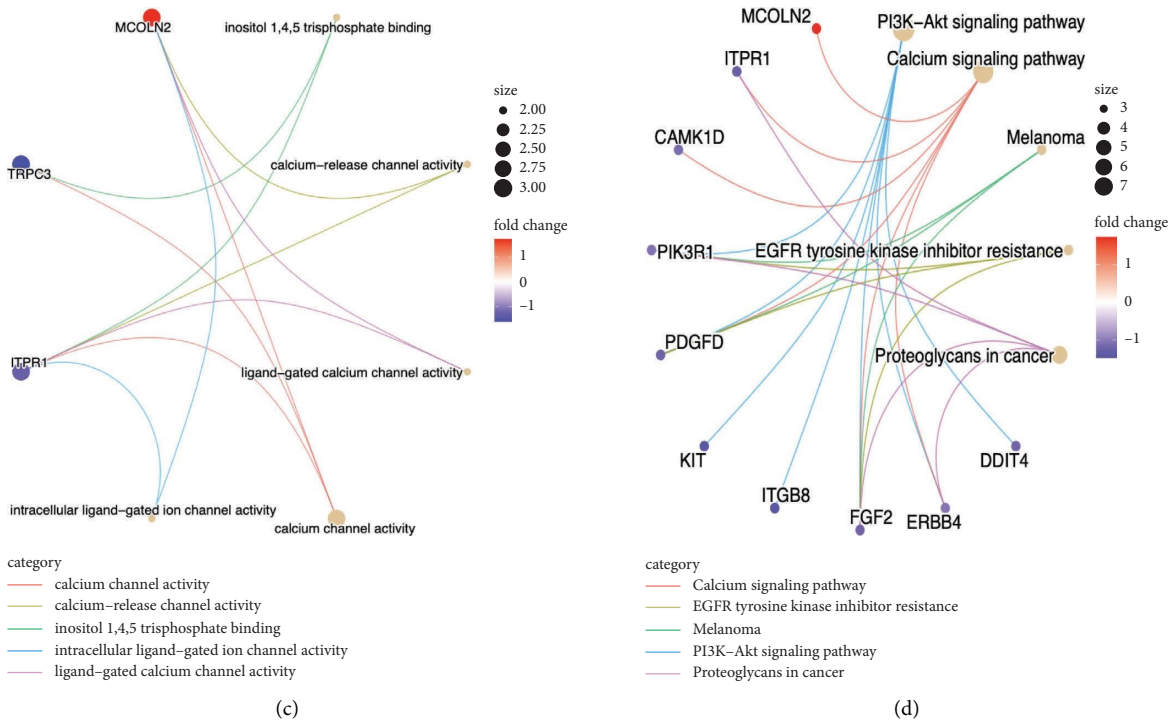

Figure 6: Cyclic diagrams of GO (BP (a), CC (b), MF (c)) and KEGG (d) enrichment. Red dots represent upregulated targeted DE-mRNAs, blue dots represent downregulated targeted DE-mRNAs, yellow circles represent mRNA-enriched functions or pathways, and the size of the circles represents the number of enriched mRNAs.

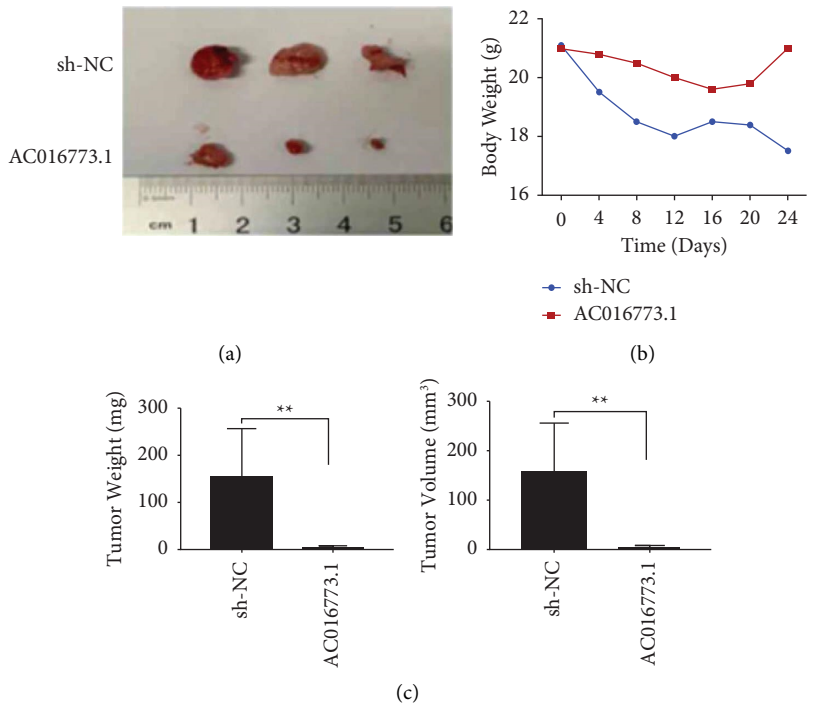

Figure 7: AC016773.1 knockdown inhibits PCa tumor growth in vivo. (a) Subcutaneous xenograft model for PC-3 cells treated as indicated and dissected tumors from sacrificed mice were shown, (b) weight changes in two groups of mice, and (c) detection of tumor volume and weight in a xenograft mouse model established by subcutaneous injection of sh control transfected and sh-AC016773.1 transfected PC3 cells.

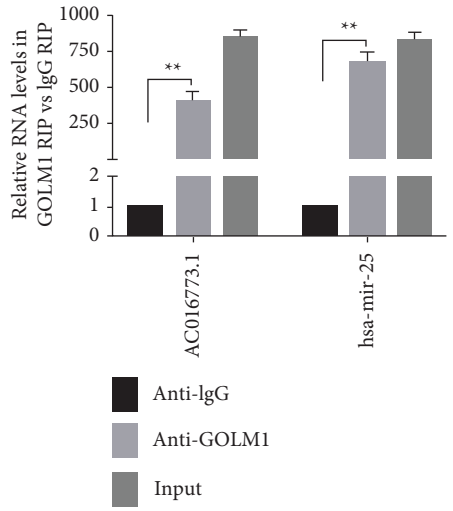

Figure 8: RIP experiments were performed in PC3 cells, and the coprecipitated RNA was subjected to RT-qPCR for analysis of AC016773.1 and hsa-mir-25 expression. $^{**}P < 0.01$ vs. IgG.

mRNAs were mainly related to calcium signaling pathway, EGFR tyrosine kinase inhibitor resistance, melanoma, PI3K–Akt signaling pathway, and proteoglycans in cancer.

EZH2 (enhancer of zeste 2 polycomb repressive complex 2 subunit) encodes a member of the polycomb-group (PcG) family [29]. PcG family members form polymer-protein complexes, which are involved in maintaining the transcriptional inhibition of genes in continuous cell generations [30]. In the past two decades, more and more evidence has shown that EZH2 mutation or overexpression exists in many tumors (including PCa) [31]. Varambally et al. [32] found that ectopic expression of EZH2 in prostate cells induces transcriptional suppression of specific gene queues. In addition, EZH2 mRNA and EZH2 protein expressions were upregulated in metastatic PCa, and the higher the expression of EZH2, the worse the prognosis of localized PCa. This suggested that dysexpression of EZH2 may be involved in the progression of PCa and is a potential marker to distinguish localized PCa from metastatic PCa. The protein encoded by GOLM1 (Golgi membrane protein 1) is a type II Golgi transmembrane protein, which is responsible for synthesizing protein in the rough endoplasmic reticulum and assisting in the transport of protein goods through Golgi [33]. Yan et al. [34] conducted real-time RT-PCR, western blotting, and immunohistochemical (IHC) analysis, as well as in vitro and in vivo functional experiments, and found that GOLM1 expression was upregulated in all grades and stages of PCa, and GOLM1 acted as a key oncogene by promoting cell proliferation, migration and invasion, and inhibiting cell apoptosis in PCa. Chen et al. [35] found elevated levels of LINC00992 and GOLM1 detected in PCa tissues and cells. LINC00992 interacts with miR-3935 and is negatively regulated to enhance the expression of GOLM1 in PCa cells. In addition, LINC00992 depletion inhibited tumor growth in vivo, offset by enhanced GOLM1 expression. Through experiments, it was found that the expression of AC016773.1 is significantly upregulated in PCa tissues and cell lines. Knockout AC016773.1 damaged tumor growth in animal models. Biological functional analysis shows that overexpression of AC016773.1 significantly promotes cell proliferation and migration, while knocking down AC016773.1 inhibits cell proliferation and migration.

In this study, the differential expression matrixes of lncRNA, miRNA, and mRNA were obtained, the ceRNA (lncRNA-miRNA-mRNA) regulatory network was constructed, and the differential expression of RNAs in the regulatory network and its correlation with survival prognosis were analyzed. Finally, GO function and KEGG pathway enrichment analysis were performed for DE-mRNAs in PCa. Our results will contribute to the further understanding of the molecular pathogenesis of PCa and the development of potential prognostic markers and drug targets, which may provide valuable clinical direction for targeted therapy of PCa patients. There are some limitations to this study, however, such as the lack of in vitro and in vivo experimental verification of large samples and the lack of different clinical classifications and stagings. Further research and exploration will be pursued in these directions in the future.

Data Availability

The dataset used and/or analyzed during this study is available from the corresponding author.

Conflicts of Interest

The authors declare that they have no conflicts of interest.

Authors' Contributions

Hongliang Wu wrote the original draft. Sheng Wang and Zhijun Chen collected raw data. Shuai Yang and Wenyan Sun performed statistical and bioinformatics analyses. Han Guan supervised the study.

Acknowledgments

The authors thank the TCGA database for providing the data. This work was supported by the 2021 Bengbu Municipal Science and Technology Innovation Guidance Project, the relationship and role of mir-133a and TGFBR1 in the malignant progression of prostate cancer (No. 20210341) and 2023 Anhui Province University Scientific Research Projects, Nomogram model of genetic variation of long noncoding gene meg3 predicts the occurrence, development, and prognosis of prostate cancer (No. 2023ah051942).

Supplementary Materials

Supplementary Document 1: 492 samples in the PCA group and 51 samples in the normal untreated group (nu). Supplementary Document 2: 2010 DE-lncRNAs comparison information and 75 lncRNAs and miRNAs interaction pairs through the miRcode database and Perl script. Supplementary Document 3: 34 pairs of de mRNAs and de miRNAs and 75 pairs of de lncRNAs and de miRNAs were obtained by Perl script. (*Supplementary Materials*)

References

[1] Q. Chen, Y. Li, X. Zhou, and R. Li, "Oxibendazole inhibits prostate cancer cell growth," *Oncology Letters*, vol. 15, no. 2, pp. 2218–2226, 2018.

[2] S. Hong, B. Song, H. Lee, and M. Lee, "Outcomes of men aged ≤50 years treated with radical prostatectomy: a retrospective analysis," *Asian Journal of Andrology*, vol. 21, no. 2, pp. 150–155, 2019.

[3] S. K. Rhie, A. A. Perez, F. D. Lay et al., "A high-resolution 3D epigenomic map reveals insights into the creation of the prostate cancer transcriptome," *Nature Communications*, vol. 10, no. 1, p. 4154, 2019.

[4] S. S. Dasari, M. Archer, N. E. Mohamed, A. K. Tewari, M. G. Figueiro, and N. Kyprianou, "Circadian rhythm disruption as a contributor to racial disparities in prostate cancer," *Cancers*, vol. 14, no. 20, p. 5116, 2022.

[5] T. Feng, C. Song, Z. Wu, K. Zhao, and S. Ye, "Role of lncRNA MIAT/miR-361-3p/CCAR2 in prostate cancer cells," *Open Medicine*, vol. 17, no. 1, pp. 1528–1537, 2022.

[6] Y. Wan, R. Halter, A. Borsic et al., "Hsa_circ_0088233 alleviates proliferation, migration, and invasion of prostate cancer by targeting hsa-miR-185-3p," *Frontiers in Cell and Developmental Biology*, vol. 8, Article ID 528155, 2020.

[7] Y. Wan, R. Halter, A. Borsic, P. Manwaring, A. Hartov, and K. Paulsen, "Sensitivity study of an ultrasound coupled transrectal electrical impedance tomography system for prostate imaging," *Physiological Measurement*, vol. 31, no. 8, pp. S17–S29, 2010.

[8] W. Liu, C. Zhao, Y. Huang, Y. Liu, and M. Lu, "The efficacy and molecular mechanism of the effect of schisandrin b on the treatment of erectile dysfunction," *Iranian journal of basic medical sciences*, vol. 22, no. 8, pp. 866–871, 2019.

[9] F. Tu, M. Li, Y. Chen et al., "Let-7i-3p inhibits the cell cycle, proliferation, invasion, and migration of colorectal cancer cells via downregulating CCND1," *Open Medicine*, vol. 17, no. 1, pp. 1019–1030, 2022.

[10] X. Du, D. Tian, J. Wei et al., "miR-199a-5p exacerbated intestinal barrier dysfunction through inhibiting surfactant protein D and activating NF-κB pathway in sepsis," *Mediators of Inflammation*, vol. 2020, Article ID 8275026, 10 pages, 2020.

[11] Y. Hu, X. Gu, Y. Duan, Y. Shen, and X. Xie, "Bioinformatics analysis of prognosis-related long non-coding RNAs in invasive breast carcinoma," *Oncology Letters*, vol. 20, no. 1, pp. 113–122, 2020.

[12] J. Wang, J. P. Hao, M. N. Uddin et al., "Identification and validation of inferior prognostic genes associated with immune signatures and chemotherapy outcome in acute myeloid leukemia," *Aging*, vol. 13, no. 12, pp. 16445–16470, 2021.

[13] J. Pei, Y. Wang, and Y. Li, "Identification of key genes controlling breast cancer stem cell characteristics via stemness indices analysis," *Journal of Translational Medicine*, vol. 18, no. 1, p. 74, 2020.

[14] Y. Q. Shi, W. F. Qi, and C. Y. Kong, "Drug screening and identification of key candidate genes and pathways of rheumatoid arthritis," *Molecular Medicine Reports*, vol. 22, no. 2, pp. 986–996, 2020.

[15] Y. Gan, J. Long, Y. Zeng, Y. Zhang, and Y. Tao, "lncRNA IL-17ra-1 attenuates LPS-induced sepsis via miR-7847-3p/PRKCG-mediated MAPK signaling pathway," *Mediators of Inflammation*, vol. 2022, Article ID 9923204, 17 pages, 2022.

[16] K. Yang, X. F. Lu, P. C. Luo, and J. Zhang, "Identification of six potentially long noncoding RNAs as biomarkers involved competitive endogenous RNA in clear cell renal cell carcinoma," *BioMed Research International*, vol. 2018, Article ID 9303486, 13 pages, 2018.

[17] J. Guan, P. Liu, A. Wang, and B. Wang, "Long non-coding RNA ZEB2-AS1 affects cell proliferation and apoptosis via the miR-122-5p/PLK1 axis in acute myeloid leukemia," *International Journal of Molecular Medicine*, vol. 46, no. 4, pp. 1490–1500, 2020.

[18] M. Wu and Y. Zhang, "Integrated bioinformatics, network pharmacology, and artificial intelligence to predict the mechanism of celastrol against muscle atrophy caused by colorectal cancer," *Frontiers in Genetics*, vol. 13, Article ID 1012932, 2022.

[19] L. Chen, T. Zhang, S. Zhang et al., "Identification of long noncoding RNA-associated competing endogenous RNA network in the differentiation of chicken preadipocytes," *Genes*, vol. 10, no. 10, p. 795, 2019.

[20] P. W. Hook and A. S. McCallion, "Leveraging mouse chromatin data for heritability enrichment informs common disease architecture and reveals cortical layer contributions to schizophrenia," *Genome Research*, vol. 30, no. 4, pp. 528–539, 2020.

[21] F. Pala, D. Di Girolamo, S. Mella et al., "Distinct metabolic states govern skeletal muscle stem cell fates during prenatal and postnatal myogenesis," *Journal of Cell Science*, vol. 131, no. 14, 2018.

[22] C. Li, W. Yao, C. Zhao et al., "Comprehensive analysis of lncRNAs related to the prognosis of esophageal cancer based on ceRNA network and cox regression model," *BioMed Research International*, vol. 2020, Article ID 3075729, 15 pages, 2020.

[23] Z. J. Xu, J. C. Ma, J. D. Zhou et al., "Reduced protocadherin17 expression in leukemia stem cells: the clinical and biological effect in acute myeloid leukemia," *Journal of Translational Medicine*, vol. 17, no. 1, p. 102, 2019.

[24] L. Chen, Y. Dong, Y. Pan et al., "Identification and development of an independent immune-related genes prognostic model for breast cancer," *BMC Cancer*, vol. 21, no. 1, p. 329, 2021.

[25] J. Lv, Y. Zhu, A. Ji, Q. Zhang, and G. Liao, "Mining TCGA database for tumor mutation burden and their clinical significance in bladder cancer," *Bioscience Reports*, vol. 40, no. 4, 2020.

[26] W. K. Shi, Y. X. Liu, X. Y. Qiu, J. Y. Zhou, J. L. Zhou, and G. L. Lin, "Construction and validation of a novel Ferroptosis-related gene signature predictive model in rectal Cancer," *BMC Genomics*, vol. 23, no. 1, p. 764, 2022.

[27] B. Zhou, H. Song, W. Xu, Y. Zhang, Y. Liu, and W. Qi, "The comprehensive analysis of hub gene ARRB2 in prostate cancer," *Disease Markers*, vol. 2022, Article ID 8518378, 16 pages, 2022.

[28] M. Knura, W. Garczorz, A. Borek et al., "The influence of anti-diabetic drugs on prostate cancer," *Cancers*, vol. 13, no. 8, p. 1827, 2021.

[29] J. Wang, L. Hua, M. Guo et al., "Notable roles of EZH2 and DNMT1 in epigenetic dormancy of the SHP1 gene during the progression of chronic myeloid leukaemia," *Oncology Letters*, vol. 13, no. 6, pp. 4979–4985, 2017.

[30] Y. Ruan, H. Xu, X. Ji, and J. Zhao, "BLM interaction with EZH2 regulates MDM2 expression and is a poor prognostic biomarker for prostate cancer," *American Journal of Cancer Research*, vol. 11, no. 4, pp. 1347–1368, 2021.

[31] S. H. Park, K. W. Fong, E. Mong, M. C. Martin, G. E. Schiltz, and J. Yu, "Going beyond Polycomb: EZH2 functions in prostate cancer," *Oncogene*, vol. 40, no. 39, pp. 5788–5798, 2021.

[32] S. Varambally, S. M. Dhanasekaran, M. Zhou et al., "The polycomb group protein EZH2 is involved in progression of prostate cancer," *Nature*, vol. 419, no. 6907, pp. 624–629, 2002.

[33] R. Xu, J. Ji, X. Zhang et al., "PDGFA/PDGFRα-regulated GOLM1 promotes human glioma progression through activation of AKT," *Journal of Experimental and Clinical Cancer Research*, vol. 36, no. 1, p. 193, 2017.

[34] G. Yan, Y. Ru, K. Wu et al., "GOLM1 promotes prostate cancer progression through activating PI3K-AKT-mTOR signaling," *The Prostate*, vol. 78, no. 3, pp. 166–177, 2018.

[35] J. Chen, X. Liu, K. Ke et al., "LINC00992 contributes to the oncogenic phenotypes in prostate cancer via targeting miR-3935 and augmenting GOLM1 expression," *BMC Cancer*, vol. 20, no. 1, p. 749, 2020.